Structures 80 (2025) 109827

Contents lists available at ScienceDirect

Structures

journal homepage: www.elsevier.com/locate/structures

Effect of concrete properties on cyclic behavior of poorly engineered RC beam-column wall joint

Amedeo Gregori , Lorenzo Bizzarri *, Caterina D'Agostino

Università Degli Studi dell'Aquila, Civil Environmental and Architectural Engineering Department, Via Giovanni Gronchi n.18, L'Aquila 67100, Italy

ARTICLE INFO

Keywords:
Reinforced concrete
Beam-column joint
Seismic performance
Cyclic loads tests
Nonlinear analysis
Sensitivity analysis

ABSTRACT

Post-earthquake observations have shown the reinforced concrete beam-column joints of dated structures may result in premature brittle failure during earthquakes. These critical zones transfer complex combination of forces between beams and columns and their premature failure may cause the catastrophic collapse of structures even in areas from low to moderate seismic risk. External beam-column joints (i.e., "wall" and "corner" joints) of buildings constructed without or with insufficient transverse reinforcement are often involved in this types of collapses. The aim of this study is to investigate how the structural response of RC beam-column joints is affected by several mechanical parameters of the concrete, including: compressive strength, tensile strength, Young's modulus, Poisson ratio and fracture energy in tension of the concrete. Both experimental tests and numerical models have been carried out. In particular, four RC beam-column sub-assemblies with no shear reinforcement in the joint have been designed, constructed and tested un- der cyclic loads. In particular, to reproduce the worst possible condition for the beam-column joints, no axial load was applied to the column the tests were performed with no axial load in the column. Experimental results were then compared with those predicted through numerical simulation carried out with a 3D FEM model, able to describe crack propagation in concrete. Experimental structural ductility of the tested RC frames were found surprisingly high and force-displacement numerical curves were found to match experimental ones both in terms of initial stiffness and maximum strength capacity. Sensitivities analysis carried out with respect of various concrete properties showed: (i) the frame strength capacity and ductility to increase with f_c; (ii) in case of low concrete strength classes, the collapse of RC frames is expected to be in shear mode; (iii) for high concrete strength classes the collapse of RC frames may be reached in the beam column joint in pressure-bending mode; (iiii) both the maximum strength capacity and the ductility of the RC frames increase as the concrete fracture energy increases; (iiiii) Poisson ratio and concrete tensile strength seem not to have much influence on the mechanical behavior of the RC frame.

1. Introduction

The performance of beam-column joints has long been recognized to have great influence on the behavior of RC frame structures subjected to horizontal cyclic loads [1–3]. First guidelines for the design of reinforced concrete beam-column joints were released in 1976 in the USA (ACI 352R-761 [4]) and in 1982 in New Zealand (NZS 3101:19822 [5, 6]). Buildings constructed before these standards are generally assumed to be characterized by a dangerous weaknesses of the beam-column joints due to the absence of shear reinforcement in these zones [1,7, 8]; in particular, they are expected not to have enough strength to provide shear stress transfer among the frame members [9].

Tests carried out according to the construction details of the 1960–1970s [10] showed that in structures designed to resist gravity loads only, RC beam-column joints were affected by brittle-type collapse mechanisms that can compromise stability and start the collapse of the whole structure [11]. In fact, post-earthquake investigations [12] and experimental studies [13–18] have shown that reinforced concrete joints of existing structures, built according to old building codes, often collapse "prematurely" even under moderate lateral forces. Moreover, in [19] the following 5 details were identified as critical for the RC joints designed for gravity loads only:

- little or no transverse reinforcements in the joint panels;
- discontinuous beam bottom reinforcements with short embedment length;

* Corresponding author.
E-mail address: lorenzo.bizzarri@graduate.univaq.it (L. Bizzarri).

https://doi.org/10.1016/j.istruc.2025.109827
Received 24 February 2025; Received in revised form 20 June 2025; Accepted 27 July 2025
Available online 7 August 2025

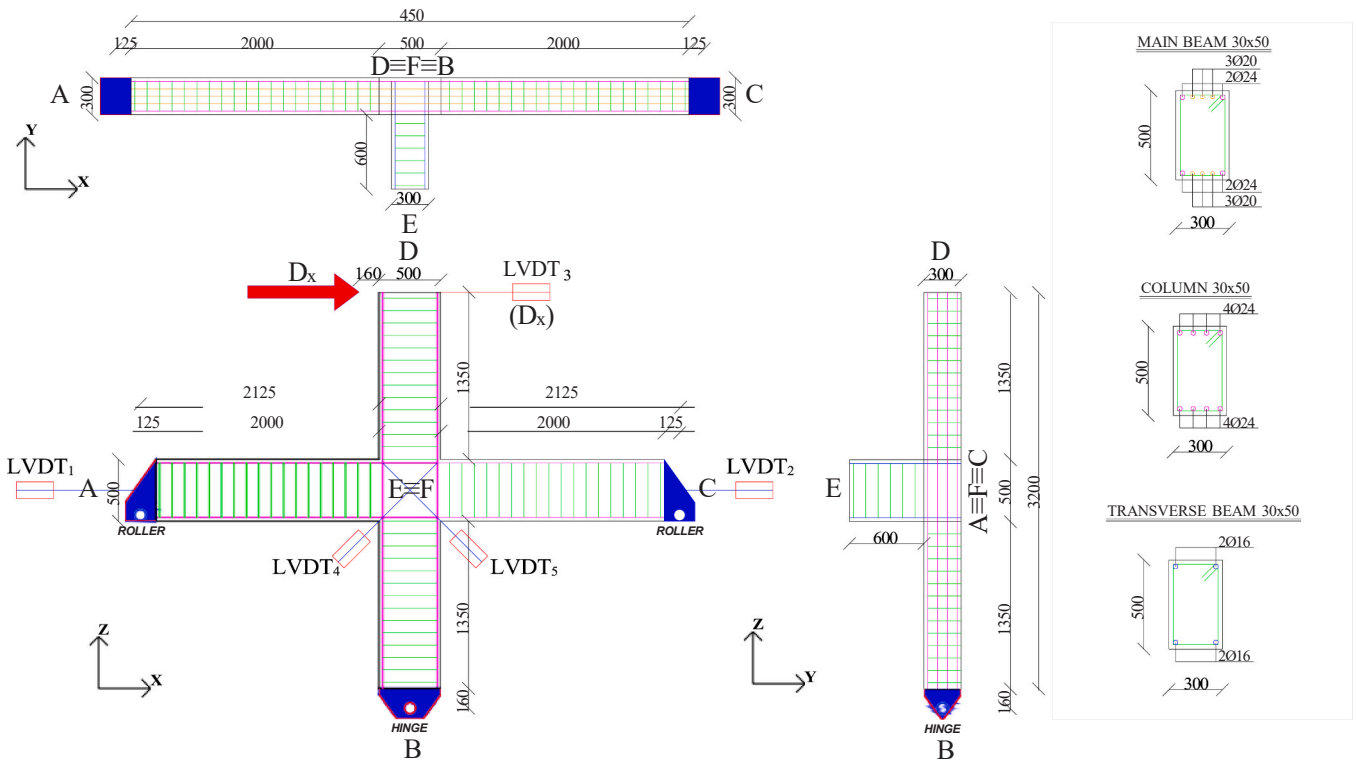

Fig. 1. Geometrical properties and reinforcement details of the specimen.

- widely spaced column ties that provided little confinement to concrete;
- lapped splices of column reinforcements just above floor levels;
- construction joints below and above the beams.

All these critical issues are today time avoided following the Capacity Design criteria [20,21] as the cardinal principle of the structural design philosophy in seismic areas. Actually, the Capacity Design ensures the structures subject to earthquakes to undergo a desired and predictable sequence of damage stages favoring a controlled dissipation of the energy introduced by the seismic forces.

Unlike other countries, the first seismic design standards establishing that stirrups of the lower column should continue in the nodal panel above, with the same spacing, were introduced in Italy only in 1997 [22]. Before [22] no nodal panel design/verification was required. Subsequent regulation issued in 2009 [23], introduced explicit design and verification of the joints, distinguishing between internal and external, fully confined and unconfined joints respectively. In [23], the joint verification is prescribed in case of the seismic assessment of existing RC buildings limiting the joint capacity to the first diagonal crack only. Unfortunately, joint verification according to [23] and to current technical standards [24] are actually so difficult to be satisfied that seismic capacity of RC buildings are strongly affected by the computed weakness of the joints.

Recent earthquakes in Italy (Molise 2002, L'Aquila 2009, Emilia 2012, central Italy 2016–2017 [25]), as well as in other earthquake-prone countries (Filippine 2024, Indonesia 2024, Russia 2024), have highlighted a great number of existing reinforced concrete structures (not matching any capacity design criteria) did not withstand seismic stresses caused by seismic forces and suffered premature

Fig. 2. View of the tested specimen.

(a) (b)

Fig. 3. (a) Details of a cracked unreinforced beam-column joint; (b) Prospective view of a cracked unreinforced beam-column joint with evidence of the dilatation of the concrete occurred in the direction perpendicular to the frame plane. Both the pictures refer to a very advanced stage of the last monotonic part of the cyclic test.

structural degradation [26] especially because of the poor-quality building materials and the not engineered constructive details. The aim of this paper is to investigate the effect of several concrete mechanical parameters on the structural behavior of RC frames with no stirrups in the beam-column joints tested under extreme cyclic loads. In particular, both experimental tests and numerical simulations have been carried out by varying several concrete mechanical parameters including: the compressive strength f_c, the tensile strength f_{ctm}, the Young's modulus E_{cm}, the Poisson factor ν and fracture energy in tension G^1. The RC beam-column joints specimens and the entire experimental setup were designed to emphasize the vulnerability of the joint and so to have the frame collapse to correspond with the failure of the joint. Indeed, no shear reinforcement was introduced in the joints to have them weaker than the beam and the columns, these latter actually designed to remain both elastic. In order to reproduce the worst load case, experimental cyclic tests have been carried out with no axial loads in the column.

Table 1
Mechanical properties of the steel bars (according to NTC018 [24]) and of the concretes (*according to CEB-FIB [30] for the numerical simulations).

Steel	f_y (MPa)	f_u (MPa)	E_s (MPa)	ν_s (-)	ε_{sy} %	ε_{su} %	
	450	540	210,000	0.29	2.14	75	
Specimen 1	f_c (Mpa)	f_{ctm} (Mpa)	E_{cm} (Mpa)	ν_c (-)	$G1$ (Nm/m2) f	h_{int} (mm)	h_{ext} (mm)
	27	2.7	29,636	0.2	0.05	20	40/80
Specimen 2	f_c (Mpa)	f_{ctm} (Mpa)	E_{cm} (Mpa)	ν_c (-)	$G1$ (Nm/m2) f	h_{int} (mm)	h_{ext} (mm)
	29.3	2.85	30,373	0.2	0.05	20	40/80
Specimen 3	f_c (Mpa)	f_{ctm} (Mpa)	E_{cm} (Mpa)	ν_c (-)	$G1$ (Nm/m2) f	h_{int} (mm)	h_{ext} (mm)
	30	2.89	30,588	0.2	0.05	20	40/80
Specimen 4	f_c (Mpa)	f_{ctm} (Mpa)	E_{cm} (Mpa)	ν_c (-)	$G1$ (Nm/m2) f	h_{int} (mm)	h_{ext} (mm)
	31	2.96	30,890	0.2	0.05	20	40/80

Finite elements models have also been developed to validate the experimental results and to carry out sensitivity analyses with respect of the above mentioned mechanical concrete parameters. Numerical results reproduced quite well the experimental force-displacement curves both in terms of initial stiffness and maximum strength capacity of the tested beam column joint sub-assemblies. Concurrently, FEM analyses showed different stress patterns to take place in the beam column joints depending on the adopted concrete strength, also resulting in variable joint failure modes, variation of compressed concrete strut width and different global ductility of the tested RC frames.

These findings represent a relatively new perspective in relation to the existing technical literature, as the width of the compressed strut is still of ten considered as a constant even in the most recent studies [27]. Therefore, this study may provide a valuable contribution toward developing more comprehensive and clearer methods for evaluating the performance of poorly RC beam-column joints.

2. Experimental setup and main test results

Four reinforced concrete beam-column frames were designed, constructed and tested to reproduce typical sub-assembly of a multi-storey reinforced concrete structure subjected to horizontal loads. In particular experimental tests were performed placing the specimen horizontally, fixing it to a strong RC floor as shown in Fig. 1 and in Fig. 2 respectively.

In particular, an hinge support was placed at the bottom end "B" of the column "DB" and a roller supports have instead located at the two beam ends (Fig. 1), so allowing for free translation and rotation in "A" and "C". The upper end "D" of the column, was connected to an electrically driven actuator by which cyclic displacement have been imposed to the specimen. It is worth to notice that ends "A","B","C" and "D" of the specimen correspond to the half-length of the beam and the column of a complete RC frame, where the inflection points are actually located when seismic loads are considered. The geometric dimensions of the specimens and their reinforcement details are shown in Fig. 1. The main beam "AC" and the column "DB" measured 300 mm × 500 mm in their cross-section. The column total height and the main beam total length measure 3200 mm and 4500 mm respectively. To better reproduce the geometry of the existing reinforced concrete frames and the confining action possibly associated with the presence of beam orthogonal to the buildings facade, a 600 mm long transverse beam "EF" (measuring 300 mm × 500 mm in cross-section) was introduced perpendicular to the main frame.

The column "DB" was reinforced with a group of 4 longitudinal steel bars measuring ϕ24 mm in diameter set on both the short sides of the

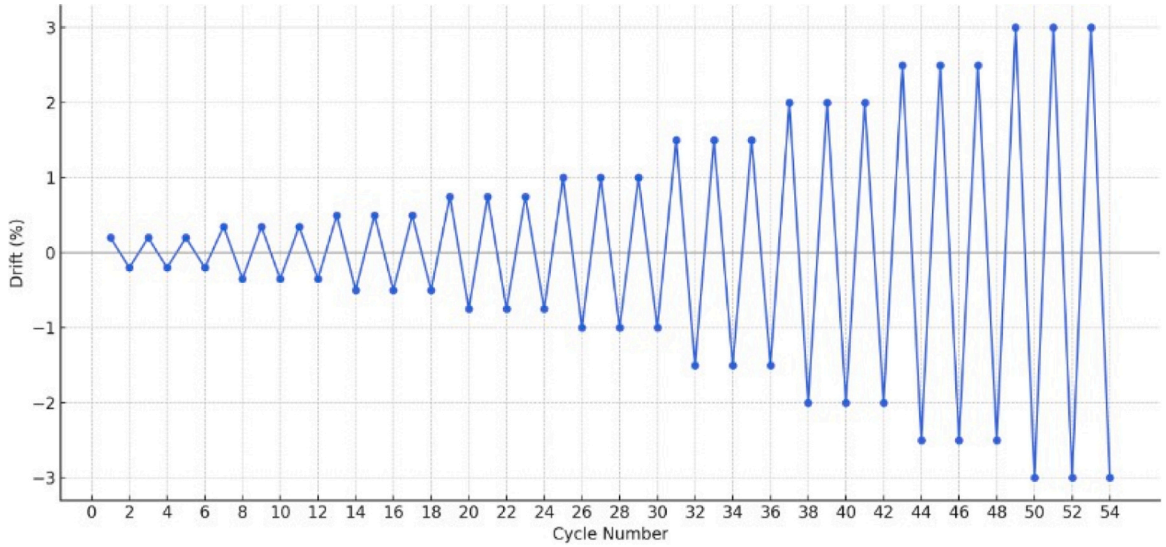

Fig. 4. Ideal standard test protocol ACI 374.1 (2005).

section. Referring to the beam "AC", 2 ϕ24 mm + 3 ϕ20 mm were introduced as longitudinal reinforcement on both the short sides of the element cross section. About the short transverse beam "EF", the longitudinal reinforcement consisted of 4 ϕ16 mm (one in each corner). Transverse reinforcement for columns and beams elements consisted of ϕ10 mm stirrups at spacing of 100 mm. No stirrups were introduced in the beam-column joint instead, so reproducing the condition frequently recognized in old existing RC buildings [28].

To measure and record the main displacements of the frame during the cyclic test [29], three linear variable displacement transducers (LVDTs) have been introduced in the positions shown in Figs. 1 and 2 respectively. In particular, one LVDT was placed at the top end "D" of the column (Fig. 2), and two LVDTs were aligned with the main beam axis, at the left end "A" and the right end "C" of the beam respectively (Fig. 2). Two Additional LVDTs were placed along the diagonals of the beam-column joint to measure its distortions. An electrically driven actuator was used to impose cyclic displacements at the end "D" of the column and a 500 kN capacity load cell was used to record the force resisted by the tested specimen.

Adopted steel rebars were characterized by a yield strength f_y = 450 MPa, while the average concretes compressive strength of the four specimens ranged from a minimum of f_c = 27 MPa to a maximum of f_c = 31 MPa as shown in Table 1.

Experimental strength values of the used concretes have been determined in accordance with UNI EN 206–1 and are reported in Table 1. Other materials mechanical properties listed in Table 1 correspond to the values assumed in the numerical simulations discusses ahead in this paper and include:

1. E_{cm}, E_s: Young's module of concrete and steel respectively;
2. f_c, f_{ctm}: compression and tensile strength of concrete;
3. f_y, f_u: yielding and ultimate strength of steel rebars;
4. G^1: tensile energy fracture of the concrete;
5. h_{int}: size of the FEM mesh adopted for the joint (see Fig. 7);
6. h_{ext}: size of the FEM mesh adopted for beam and column element external to the joint (see Fig. 7);

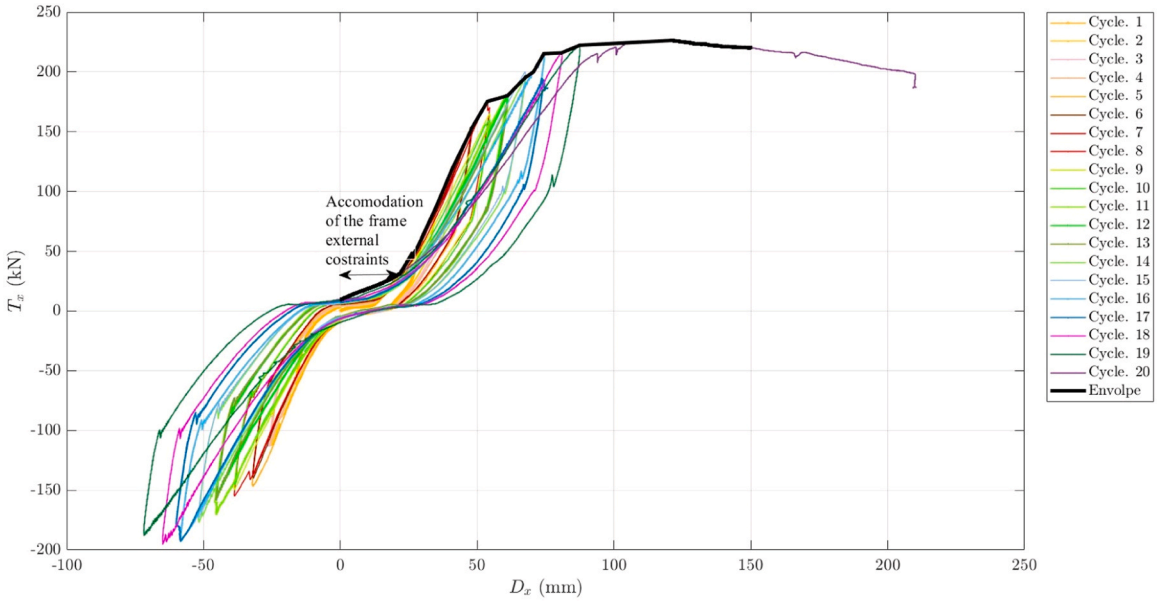

Fig. 5. Hysteresis cycles of the experimental test (Specimen 2).

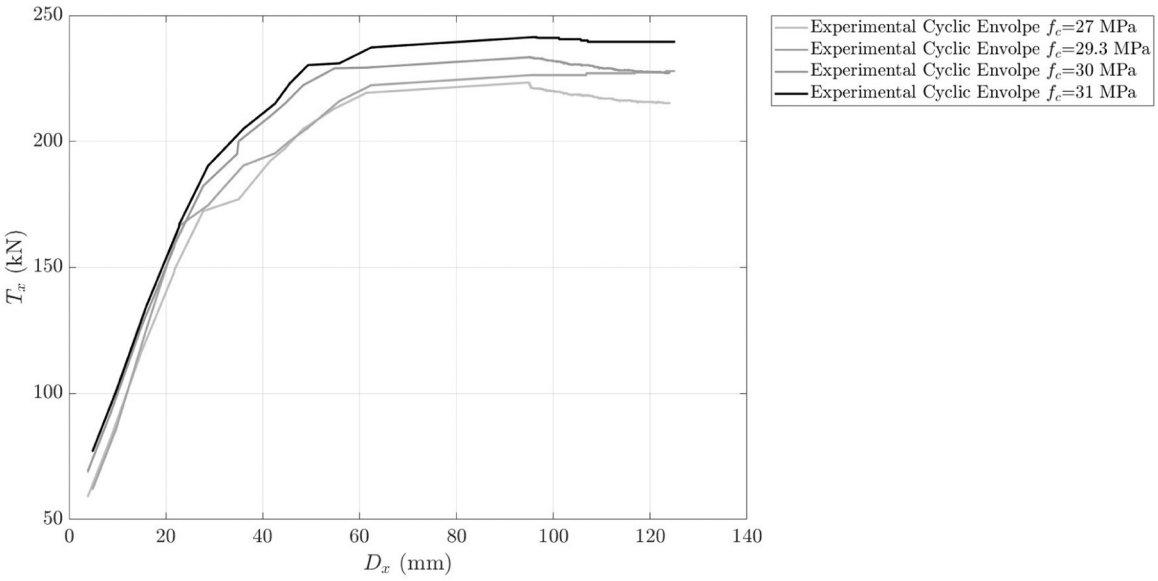

Fig. 6. Shear-displacement experimental curves: envelopes.

7. ε_{sy}, ε_{su}: deformation at the yielding strength and at the ultimate strength of the steel rebars respectively (according to a bilinear elastic-hardening response law);
8. ν_c, ν_s: Poisson's ratio of concrete and steel respectively.

The specimens were tested by imposing a precise sequence of quasi-static cyclic relative displacements (repeated at increasing amplitude) between the two ends of the column. Details of the loading protocol for all specimens were based on ACI Standard 374.1 [31] (Fig. 4).

In order to minimize the capacity of the beam-column joints no axial loads were applied to the column. In fact, axial compressive stresses transmitted in vertical direction by the column to the joint are recognized to improve the capacity of the tie-rod mechanism, as the diagonal strut becomes wider [32]. As an example of the data recorded during the experimental cyclic test, those referring to specimen number 2 have been plotted in Fig. 5. In particular, the hysteresis cycles and their envelope curve have been reported in terms of shear force T_x resisted by the frame with respect of the imposed displacement D_x.

Similarly, all the envelope curves recorded in the experimental campaign have been plotted in Fig. 6 ignoring the initial accommodation of the specimens and of the external constraints.

Experimental envelope curves plotted in the Fig. 6 show the response of the tested specimens to be similar each other. In particular, the recorded mechanical behaviour of all the RC frames highlighted the following common evidences:

- an initial settling of the constraints (initial, almost horizontal, branch of Fig. 5);
- a subsequent linear elastic response;
- a gradual reduction in stiffness for any repeated loading cycle until the maximum shear response $T_{x,MAX}$ is reached and then maintained even at very large displacements D_x (drift);
- although the beam-column joints did not include any type of shear reinforcement, all the tested specimens showed a surprisingly high structural ductility. In fact, experimental shear capacity of the frames reduced more than 15 % only at drift values larger than 4.7 %, well above the ultimate limit considered by recent building codes for modern and engineered RC frames.

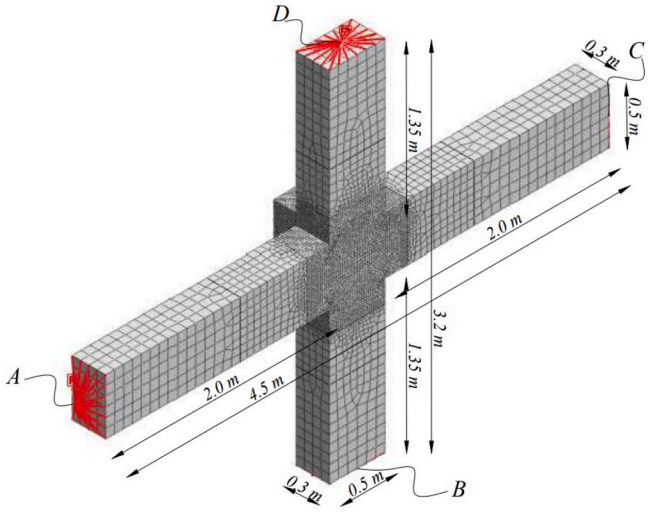

Fig. 7. Geometric dimensions of the numerical model.

3. Numerical analysis

3.1. Modeling and main analysis results

FEM models have been developed to numerically reproduce experimental cyclic tests. Fig. 7 shows the geometric dimensions of the numerical models built coherently with the real specimens and setup.

Similar to previous study carried out on RC members subjected to cyclic loads [33–38], the diffuse crack model (*"Concrete Smeared Cracked"*) has been assumed for concrete in this study as well.

In particular, consistently with references [28,37,38], the concrete behavior in compression and in tension have been assumed in accordance to models JSCE-2017 and Hordijik respectively.

To achieve an optimal balance between simulation accuracy and computational efficiency, and to enable a detailed investigation of the nonlinear behavior of the beam–column joint through sensitivity analyses, a different discretization of the RC specimen was adopted. Specifically, eight-node solid

brick elements with a maximum mesh size of 20 *mm* were used to mesh the joint region, extending up to 200 *mm* from its edges. The beam

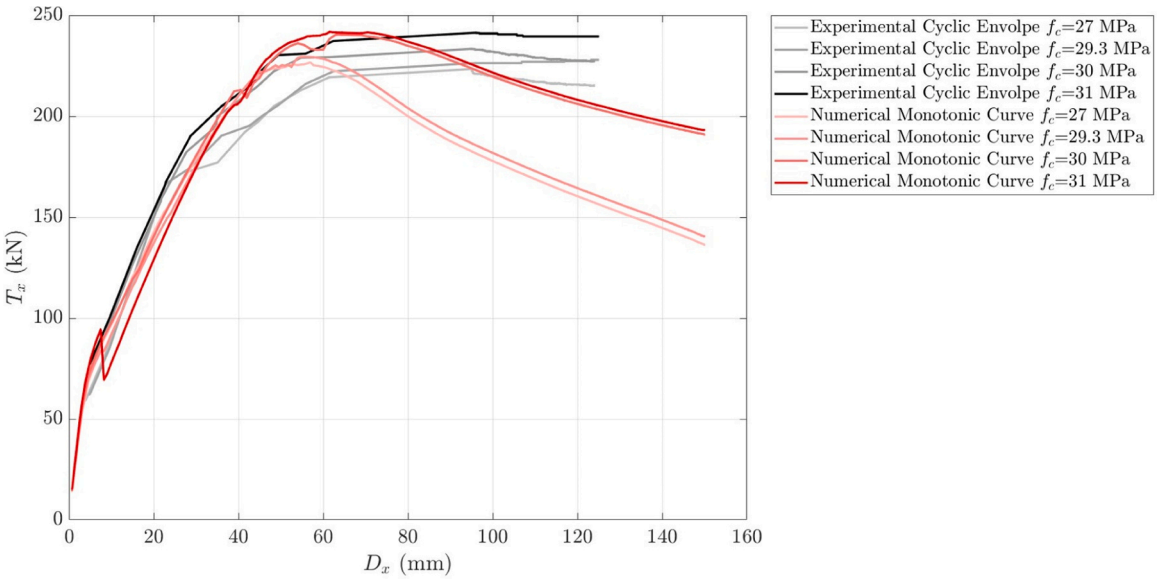

Fig. 8. Comparison between experimental envelopes of the cyclic tests and numerical monotonic curves.

and column end regions—extending 1200 *mm* and 770 *mm*, respectively—were discretized

with a coarser mesh size of 80 *mm*. The remaining central portions of the beam and column, measuring 600 *mm* and 380 *mm* respectively, were meshed with an intermediate size of 40 *mm*. These data correspond to the h parameter values indicated in Table 1. Steel bars have been modeled as two-nodes one-dimensional embedded elements characterized by a bilinear (hardening) response. Roller constraints were introduced at the ends *A* and *C* of the beam and an hinge constraint was considered at the bottom end *B* of the column. Mechanical properties assumed for all the materials are those already shown in Table 1.

To reproduce experimental tests, numerical simulations have been carried out introducing growing displacements at the top end *D* of the modeled frame and no axial forces have been applied to the column [12,39].

In Fig. 8, calculated forces-displacements curves (monotonic) are shown in comparison with experimental ones (envelopes of the experimental cyclic tests), already shown in Fig. 6.

The computed responses confirm the adopted numerical models to be quite effective in reproducing experimental results: in particular, numerical curves were found to match experimental ones both in terms of stiffness and maximum strength capacity of the specimens respectively. However numerical curves differ from the experimental ones in terms of ductility, with the capacity to maintain shear forces even at large displacements being greater in real tests than in numerical analyses.

It must be noticed that the almost perfectly plastic post-peak behavior that characterizes the experimental curves presented in this paper is common to that already presented and discussed in different research works [28,37]. We believe this type of response may be the result of the relatively small dimension of the joint, of its regular geometry and of the high transversal reinforcement found immediately outside the joint. All these favorable conditions determined the activation of a sort of mechanism fully focused into the joints region, with the

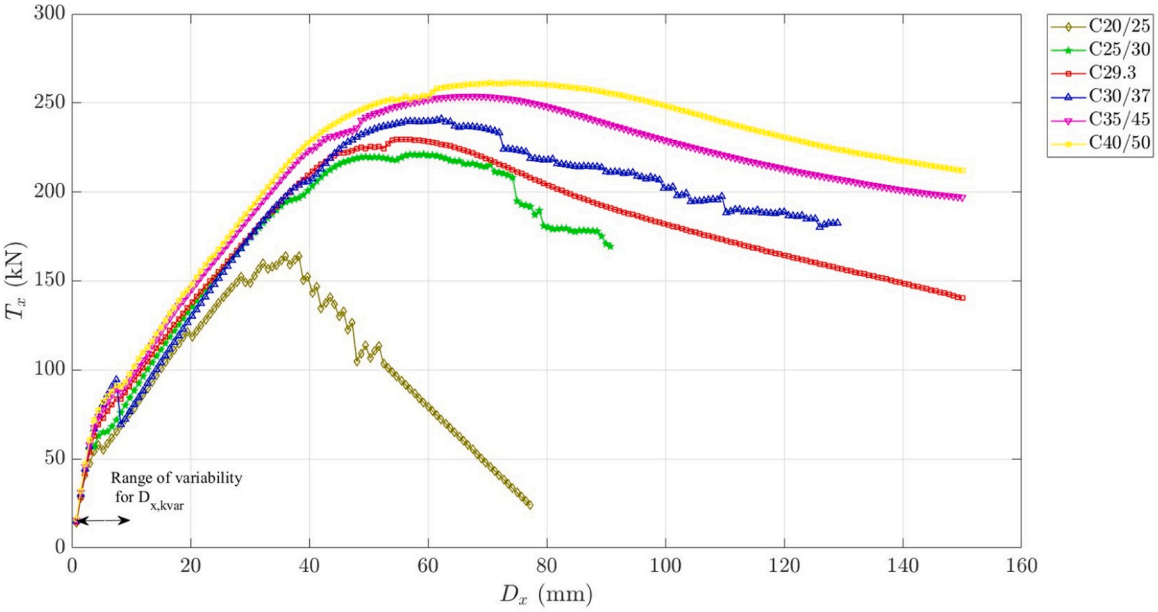

Fig. 9. Sensitivity analyses: calculated responses curves for various values of the concrete compressive strength.

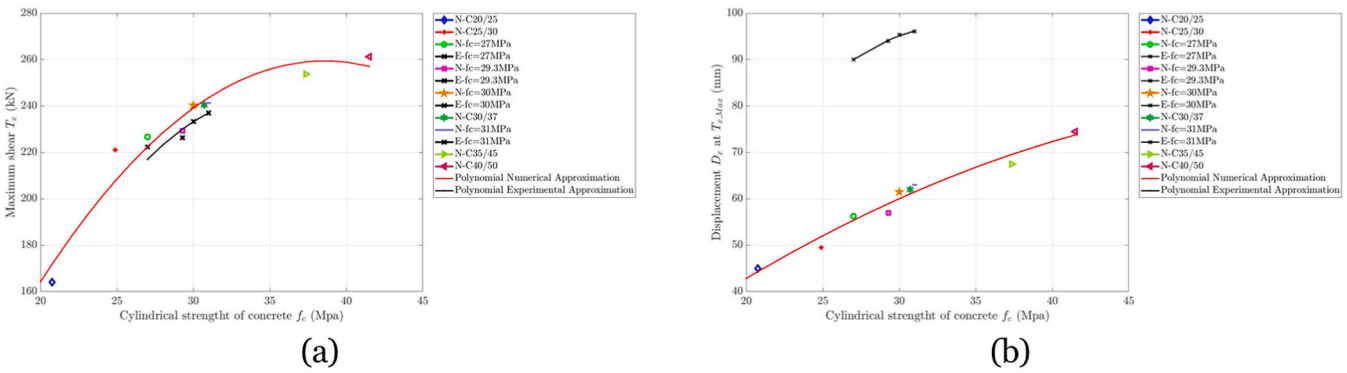

Fig. 10. (a)Relationship between the cylindrical strength of the concrete f_c and the maximum shear $T_{x,MAX}$.; (b) Relationship between the cylindrical strength of the concrete f_c and the displacement D_x at $T_{x,MAX}$.

cracked joint able to provide a stable mechanical response because of the effective border represented by the heavy and continuous longitudinal reinforcement of beams and columns. About the post-peak behavior indicated by the numerical curves, it must be observed that the slope of the softening branch is affected by the assumed concrete mechanical properties as discussed in the following sections of the paper. In particular, incremented values of the concrete deformation limits, as those corresponding, for example, to improved concrete classes, make the slope of the softening branch to reduce and the calculated post-peak response to become more similar to the experimental trend.

3.2. Sensitivity analysis

In order to investigate the variation of the computed mechanical response of the modeled frame with respect of several concrete properties, specific numerical simulations have been carried out assuming various ranges of variability for the concrete compressive strength, the concrete tensile strength, the Young's modulus, the Poisson ratio and the fracture energy of the concrete respectively.

3.2.1. Concrete compressive strength and others related properties

In particular, concrete classes ranging from C20/25 to C40/50 have been considered, and the other concrete strength related material properties have been set according to CEB FIB [30] (including the Young's Modulus E_{cm}, the compressive strength f_c and the tensile strength f_{ctm}).

The capacity curve calculated for each concrete strength class are plotted in Fig. 9.

The analysis of the data highlights both the computed maximum shear capacity ($T_{x,MAX}$) and the lateral displacement at the maximum shear ($D_{Tx,MAX}$) of the specimen to increase as the concrete class increases as shown in Fig. 10 (a) and (b) respectively.

In particular, the relation among $T_{x,MAX}$ and the assumed cylindrical concrete compressive strength f_c is plotted in Fig. 10 (a) with the calculated system capacity reducing to about 40 % (from 261 kN to 164 kN) when the concrete class is reduced from C40/50 to C20/25.

Eq. 1 represents the second order polynomial approximation functions best fitting the calculated values of $T_{x,MAX}$ versus f_c with $R^2 = 0.9447$.

$$T_{x,MAX(num)} = -0.2754\, f + 21.257\, f_c - 150.75 \quad (1)$$

Eq. 2 represents the second order polynomial approximation function best fitting the experimental values of the maximum shear recorded for the tested specimens with respect of their experimental f_c values and it is characterized by a determination coefficient $R^2 = 0.999$.

$$T_{x,MAX(exp)} = -0.4061\, f + 28.57\, f_c - 258.32 \quad (2)$$

The comparison of Eqs. 1 and 2 show the numerical models only slightly overestimate the experimental behavior of the tested specimens

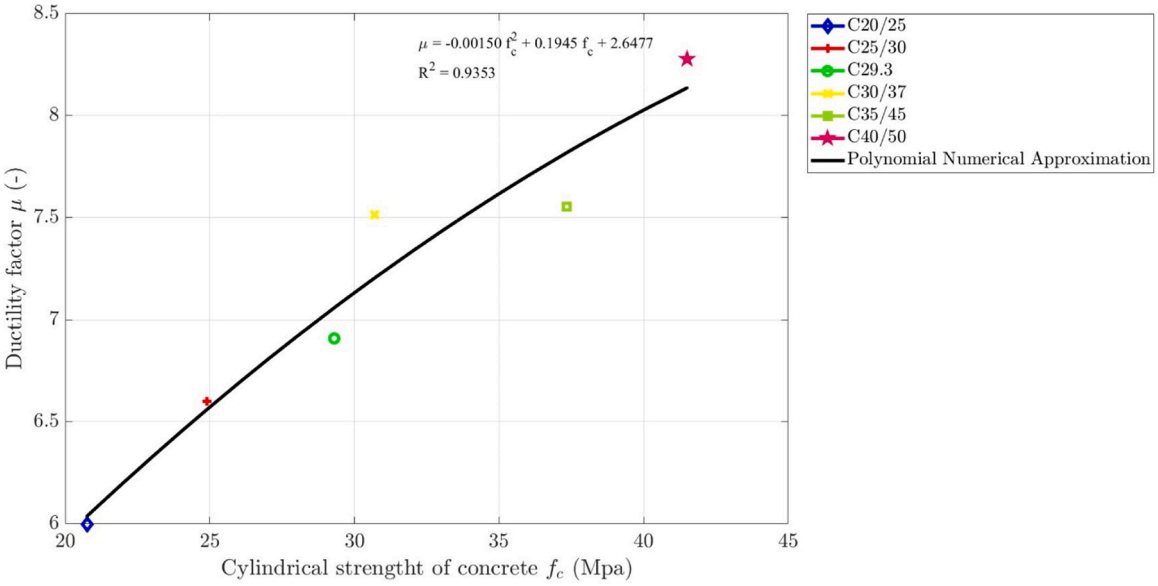

Fig. 11. Relationship between the cylindrical strength of the concrete f_c and the ductility factor μ.

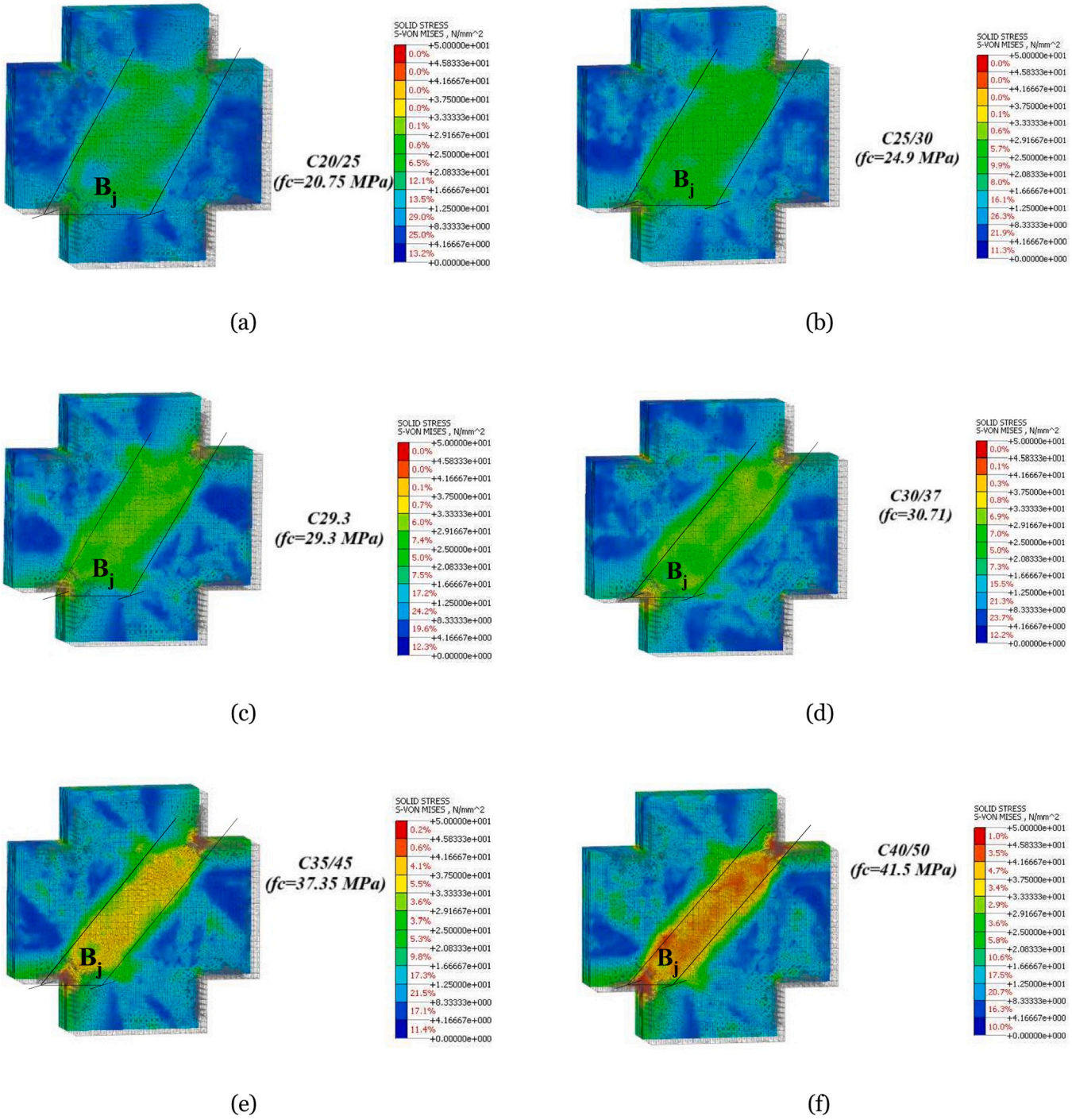

Fig. 12. Von Mises stresses (in the middle vertical plane of the joint and corresponding to the step at which $T_{x,MAX}$ is achieved) for RC joints characterized by different concrete strength classes: (a) C20/25; (b) C25/30; (c) C29.3; (d) C30/37; (e) C35/45; (f) C40/5.

in terms of maximum shear response $T_{x,MAX}$ versus f_c.

In Fig. 10 (b) the values D_x of the displacement corresponding to the values of the maximum shear $T_{x,MAX}$ are plotted with respect of the concrete strength f_c assumed in the calculation, showing D_x values to increase at increasing f_c.

Eq. 3 represents the second order polynomial approximation function best fitting calculated data of $D_{Tx,MAX}$ with respect of the assumed concrete class f_c ($R^2 = 0.9673$).

$$D_{Tx,MAX(num)} = -0.0244\, f + 2.9402\, f_c - 6.2183 \quad (3)$$

The second order polynomial approximation function computed for the experimental values $D_{Tx,MAX}$ obtained for real tests is instead represent by the Eq. 4 and it is characterized by a determination coefficient of $R^2 = 0.9956$.

$$D_{Tx,MAX(exp)} = -0.1686\, f + 11.321\, f_c - 92.758 \quad (4)$$

The comparison among Eqs. 3 and 4, both plotted in Fig. 10 (b), highlights that numerical models tends to underestimate the behavior of the experimental specimens in terms of displacements with calculated $D_{Tx,MAX}$ values representing about 60 % of the corresponding experimental ones for the same concrete class.

The failure of RC beam-column joints is generally considered to be

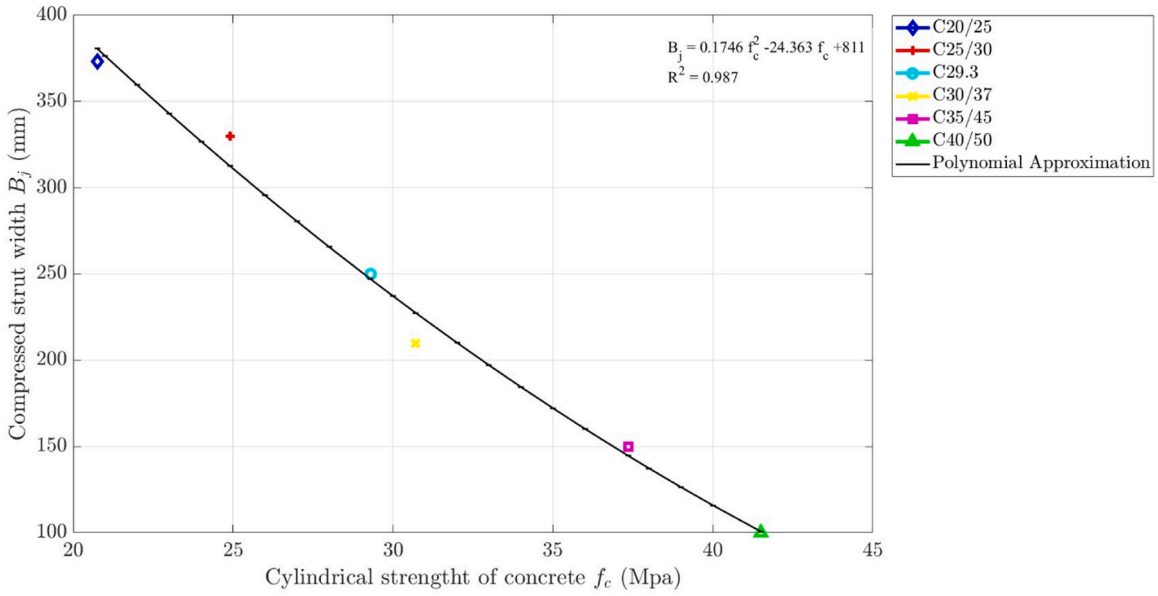

Fig. 13. Compressed strut width in the middle of the joint as the concrete class changes.

highly brittle. Defining an appropriate ductility factor μ, as done in Eq. 5, allows to better compare the performance of RC frames even in case unreinforced beam-column joints. Experimental evidences (Fig. 6) and values of μ obtained from numerical simulation as well (Figs. 11, 17, 21, 22), actually prove the ductility of the RC frames in which beam-column joints do not include any specific shear reinforcement, to be significant. This may suggest the adoption of proper behavior factors in the seismic assessment of the existing RC structures so far considered very brittle instead. In order to analyze the post-peak behavior response of the specimens, numerical values of the ductility factor μ defined by Eq. 5 have been calculated and compared [40,41].

$$\mu = ({}^{D}x,85\% - {}^{D}x,kvar)/{}^{D}x,kvar \tag{5}$$

In equation 5, $D_{x,85\ \%}$ represents the displacement at which the shear response of the frame reduces to 85 % of the maximum shear $T_{x,MAX}$ and $D_{x,kvar}$ represents the displacement at which a first significant stiffness variation is noticed along the initial elastic branch of the response curve of the specimen (see Fig. 9).

Calculated values of μ have been plotted in Fig. 11 with respect of the cylindrical concrete compressive strength values f_c. The corresponding polynomial approximation curve is represented by Eq. 6 and fits quite well the data of μ versus f_c with $R^2 = 0.9353$.

$$\mu = -0.0015\, f^2 + 0.1945 f_c + 2.6477 \tag{6}$$

Data reported in Fig. 11 show that as the concrete class increases the ductility factor μ also increases, ranging from a minimum value of $\mu = 6$ (calculated for the concrete class C20/25) to a maximum of $\mu = 8.27$ (calculated for the concrete class C40/50).

3.2.2. Stress distribution in the beam-column joint

Numerical analyses carried out with FEMs allowed to compute the stress distribution in the RC beam-column joint, and main results are graphically illustrated in Figs. 12, 13 and 14 respectively.

In particular, computed Von Mises stresses (in the middle vertical plane of the joint) corresponding to the step analyses at which $T_{x,MAX}$ is achieved, are plotted in the Fig. 12 for RC joints characterized by different con- crete strength classes. Images in Fig. 12 show that in case of low concrete strength values, the higher stresses are concentrated along the beam-column joint diagonal and the compressed strut width is significant. In case of higher f_c values, the largest stresses are focused outside of the beam-column joint, just at the beginning of the elements converging in it, and the compressed strut in the joint is slimmer. This makes believes the system failure mode to depend from the assumed value for f_c: with probable shear failure occurring in the beam-column joint in case of low f_c, and plastic hinges forming in the beams or columns when higher f_c values are considered instead.

In particular, Fig. 12 makes graphically clear that the compressed strut width B_j varies with respect of the considered concrete strength class f_c and plotting data of B_j versus f_c (Fig. 13) a second order polynomial regression is determined (Eq. 7) with a coefficient $R^2 = 0.987$.

$$B_j = 0.1746\, f^2 - 24.363\, f_c + 811 \tag{7}$$

The graph in Fig. 13 highlights how the compressed strut width B_j decreases as the concrete class increases f_c, reducing to almost 26 % of the original value when the assumed concrete compressive strength is doubled, with $B_j = 373\ mm$ (calculated for the concrete class C20/25) reducing to about $B_j = 100\ mm$ (calculated for a concrete class C40/50). These findings are relatively new with respect of the know technical literature, since the compressed strut width continue to be considered a constant even in most recent research work [27]. For this reason the present study may offer a contribution to the development of more complete and clearer approaches for the verification of poorly RC beam-column joint.

In Fig. 14, stresses acting on the reinforcing steel bars at a step analysis at which $T_{x,MAX}$ is reached are plotted for RC joints characterized by different values of the concrete compressive strength f_c. The plots highlight the largest stresses are always located in the longitudinal reinforcement of the beam near the joint. Moreover, it must be noted that only in case of the RC beam-column joint made with concrete class C20/25 the reinforcing bars did not yield while in all the other cases longitudinal reinforcement of the beam near the joint always plasticized. This result highlights that plastic hinges may

actually form on beams although no stirrups are introduced in the RC beam-column joints especially in case concrete compressive strength f_c is assumed above a given minimum value.

(b) C25/30; (c) C28/35; (d) C30/37; (e) C35/45; (f) C40/50.

3.2.3. Tensile fracture energy G^1

Additional FEMs analyses were performed to investigate the effect of other concrete mechanical parameters on the response of the RC beam-column joint. In particular, mechanical parameters considered in this section include the tensile fracture energy G^1, tensile strength f_t and

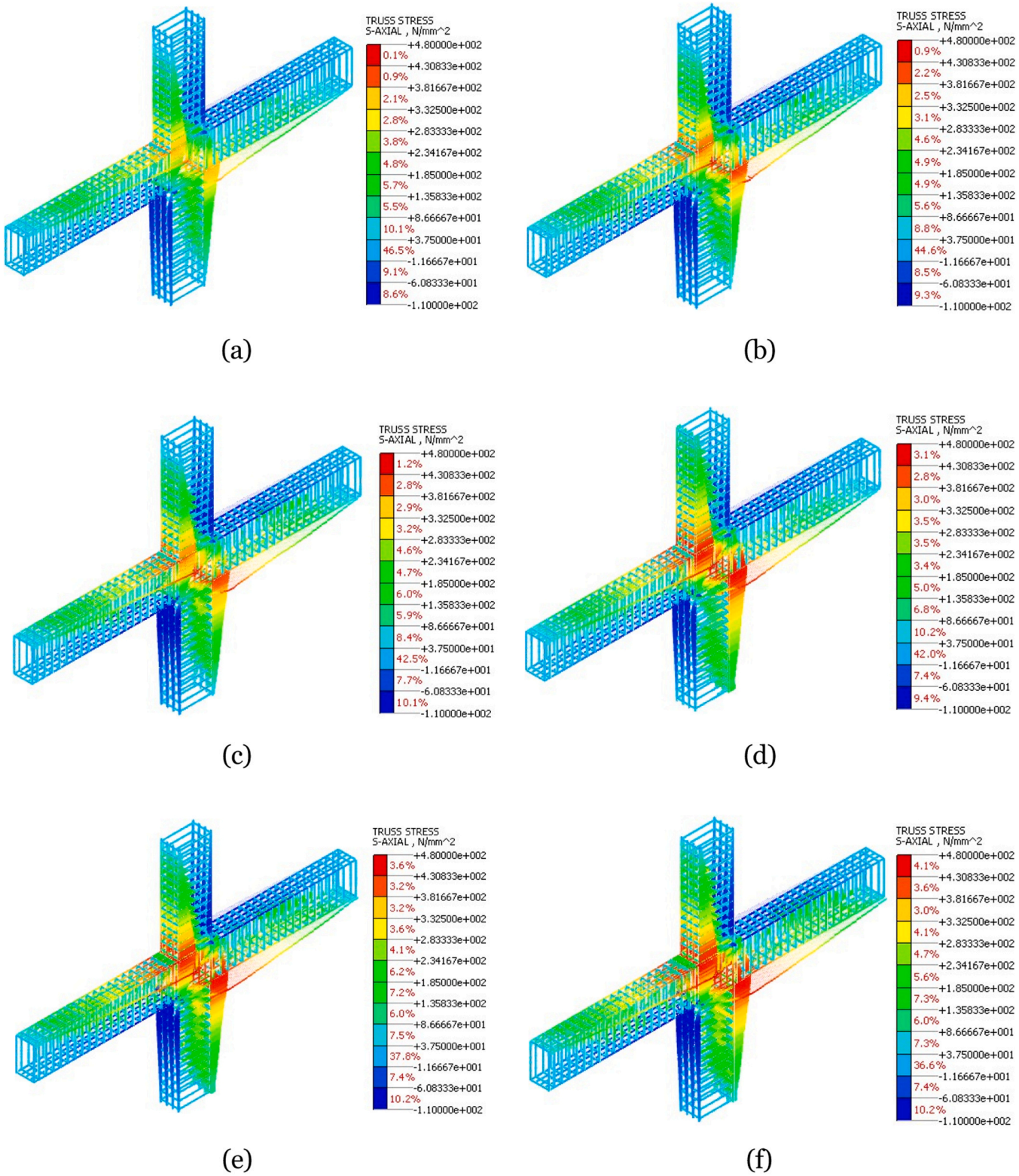

Fig. 14. Axial truss stresses of reinforcements as the concrete class changes: (a) C20/25;.

Poisson's coefficient ν.

As previously done, the *Concrete Smeared Cracked* model was assumed. According to it, cracking originates when the maximum principal stress at a point exceeds the tensile strength of the material, and that cracking is concentrated at integration points inside the elements, where the tension-softening relationship is modified to account for the consequent decrease in stiffness and strength. The crack formation process is governed by the shape of tension-softening diagram and by the value assumed for fracture energy [1] (divided by h), this latter graphically representing the area under the constitutive stress-strain curve adopted in tension and corresponding to the energy dissipated to create a crack with unit area (Fig. 15).

The dependence of both the maximum shear strength capacity $T_{x,MAX}$ and the ductility factor μ of the RC beam-column joint with respect of the

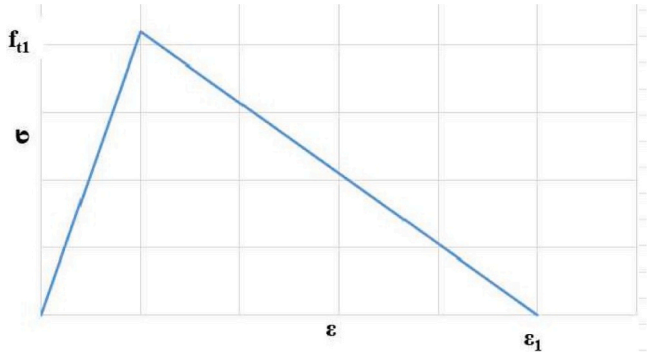

Fig. 15. Constitutive stress-strain relationship adopted for the behavior of concrete in tension.

values assumed for the fracture energy in tension have been analyzed making G^1 varying in the range $0.025 \div 0.5\ N/mm$. Data plotted in Fig. 16 show the maximum shear strength capacity $T_{x,MAX}$ to increase as G^1 increases, with the Eq. 8 representing the logarithmic approximation law best fitting the calculated results of $T_{x,MAX}$ versus G^1 with $R^2 = 0.873$:

$$T_{x,MAX} = 10.791 ln(G^1) + 255.42 \quad (8)$$

Values of μ (calculated according to Eq. 5) resulting from FEM analyses carried out assuming different G^1 values are plotted in Fig. 17. The polynomial approximation law corresponding to Eq. 9 and represent-ing the best fitting curve for data of μ versus G^1 ($R^2 = 0.977$) has also been plotted showing the ductility of the system μ clearly increases as G^1 increases, since more energy is absorbed by the material before a fracture starts to propagate and so the whole frame can sustain larger loads at larger displacements.

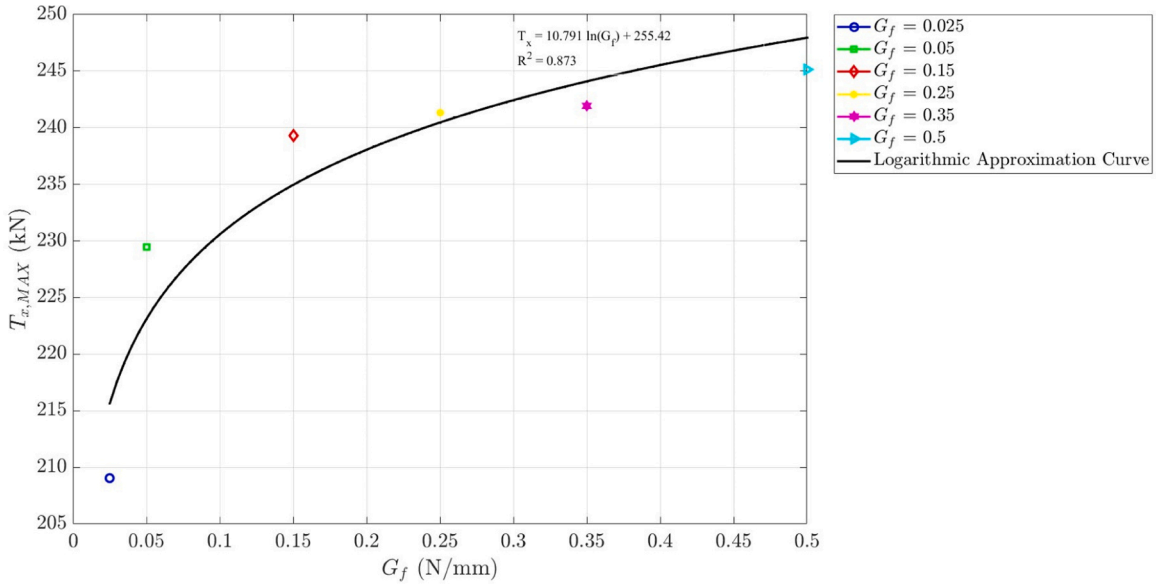

Fig. 16. Relationship between the fracture energy $G1$ and the maximum shear strength $^{T}x,MAX$.

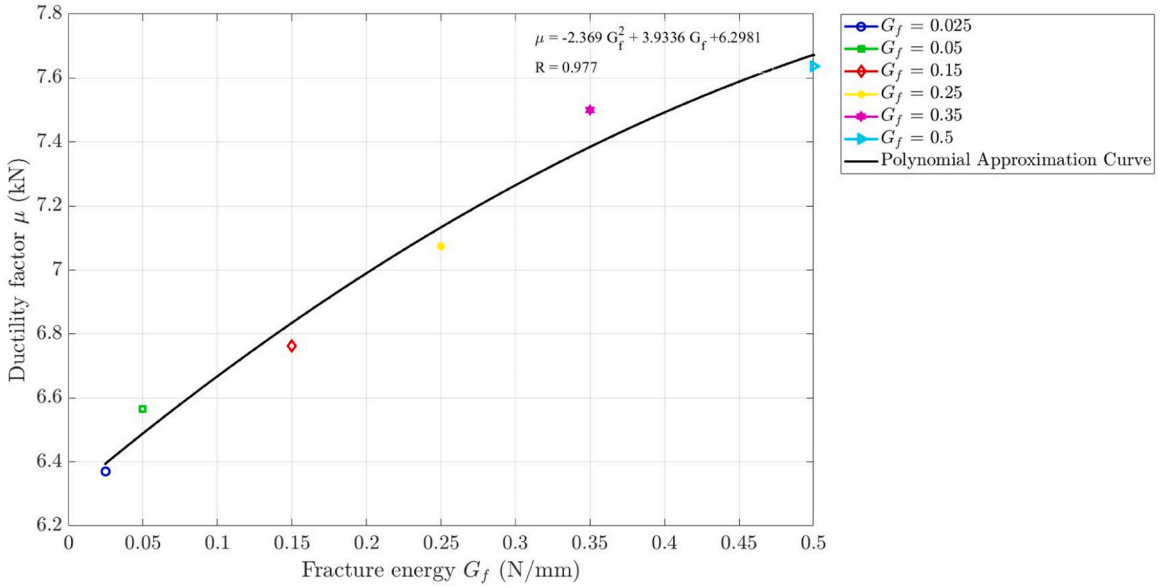

Fig. 17. Relationship between the fracture energy $G1$ and the ductility factor μ.

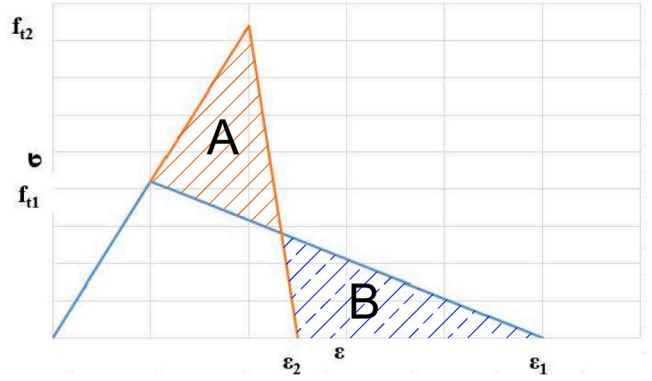

Fig. 18. Constitutive stress-strain relationship adopted for the behavior of concrete in tension: when an incremented value of the concrete tensile strength is considered (f_t2 in place of f_t1) the maximum allowed deformation reduces (from $\epsilon 1$ to $\epsilon 2$).

$$\mu = -2.369G^{1\ 2} + 3.9336G^{1} + 6.2981 \quad (9)$$

3.2.4. *Concrete tensile strength f_t and Poisson ration ν*

In previous sections of the paper, very small variation of the concrete tensile strength has been assumed in the analyses as consequence of the variation assumed for other concrete properties, mainly the concrete compressive strength f_c, from which f_{ctm} depends. In this new section of the paper, different values of the concrete tensile strength f_t have been assumed (in the range $1.4 \div 5.7\ N/mm^2$) keeping the others material properties constant. In particular, since the value of $G_f = 0.5\ N/mm$ has been fixed, to higher f_t values more brittle behaviors in tension correspond. This is graphically explained in Fig. 18 in which the "constant G_f criteria" imposes the dashed areas A and B to be equivalent each other, so that the maximum deformation allowed in tension has to be lower in case of concretes characterized by larger tensile strength values. Because of this, the initial cracking is posticipated when higher f_t values are assumed (as shown in Fig. 19) and some differences are noticed also in terms of crack distribution and crack width at the same displacement D_x, as qualitatively shown in Fig. 20. Referring to the global performance of the analyzed RC frames (both in terms of maximum shear capacity and structural ductility) data plotted in Fig. 21 show the values of $T_{x,MAX}$and those of μ not to depend on the values assumed for the concrete tensile strength f_t. The same was evident also from Fig. 19 in which all the curves reached similar values of $T_{x,MAX}$ and almost overlap each other in the softening post-peak branch of the calculated responses.

Data plotted in graph of Fig. 21 show the maximum shear capacity $T_{x,MAX}$ do not depend from the values of the concrete tensile strength assumed in the numerical analyses of this study and made to vary from $1.4\ N/mm^2$ to $5.7\ N/mm^2$, by keeping constant $G^1 = 0.5\ N/mm$. In

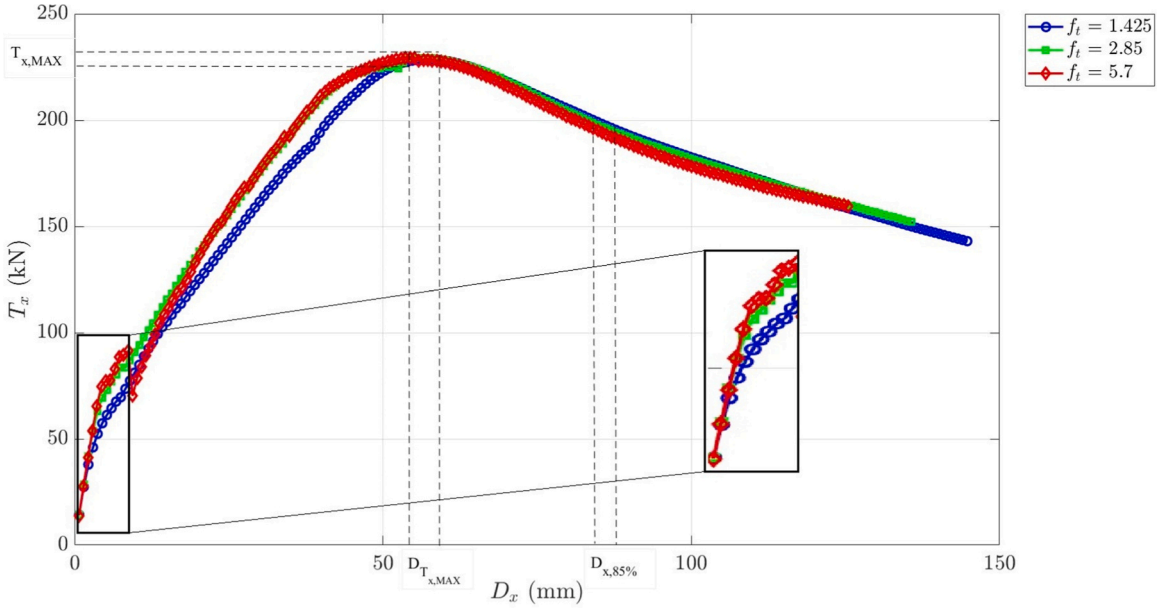

Fig. 19. Numerical curves corresponding to different concrete tensile strength values f_t. No significant variations are noticed in terms of $T_{x,MAX}$, $D_{Tx,MAX}$ and D_x,85 %, and so in terms of μ.

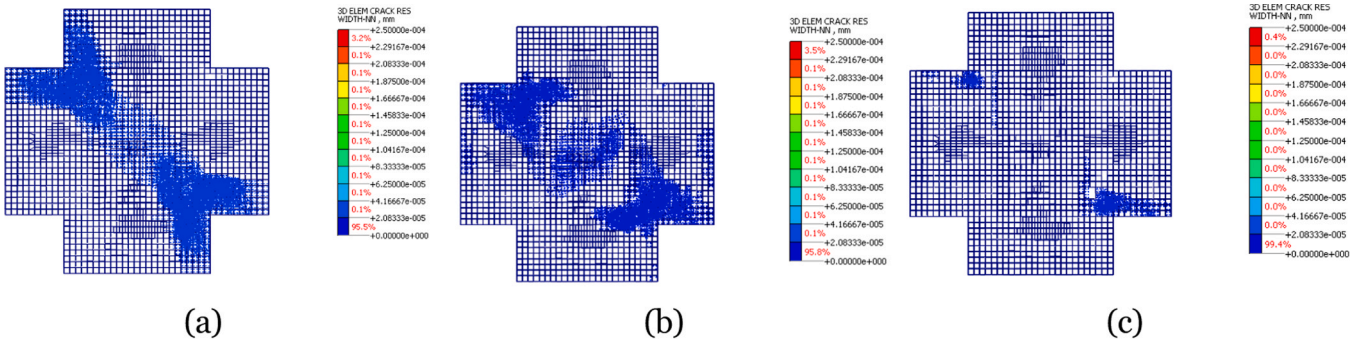

Fig. 20. Crack width (for a displacement $D_x = 8\ mm$) computed for various concrete tensile strength: (a) $f_t = 1.425\ N/mm2$; (b) $f_t = 2.85\ N/mm2$; (c) $f_t = 5.7\ N/mm2$.

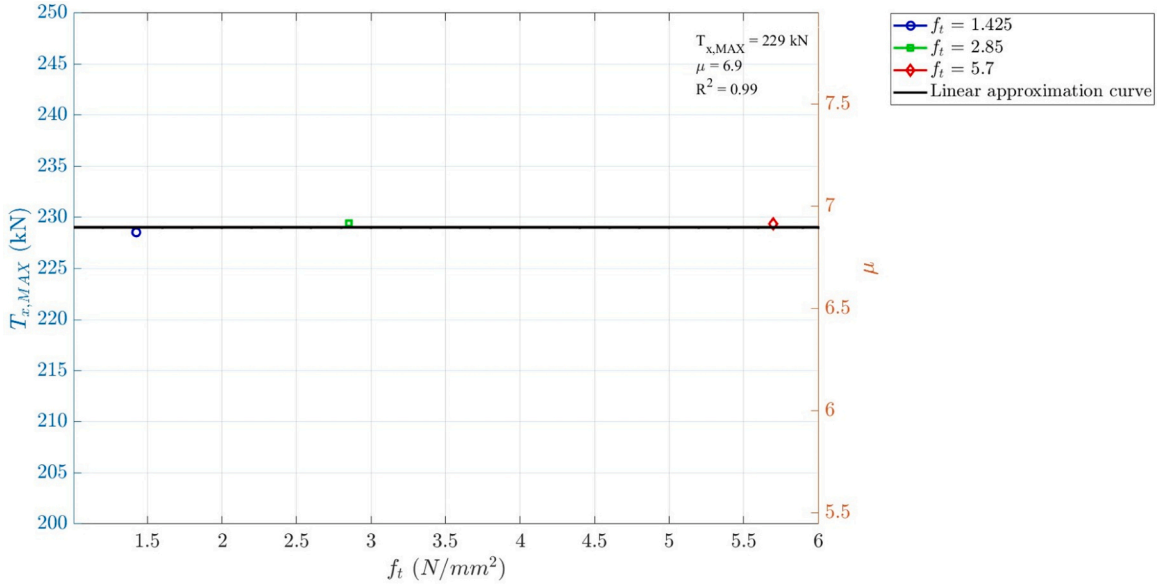

Fig. 21. Sensitivity analysis of concrete tensile strength f_t.

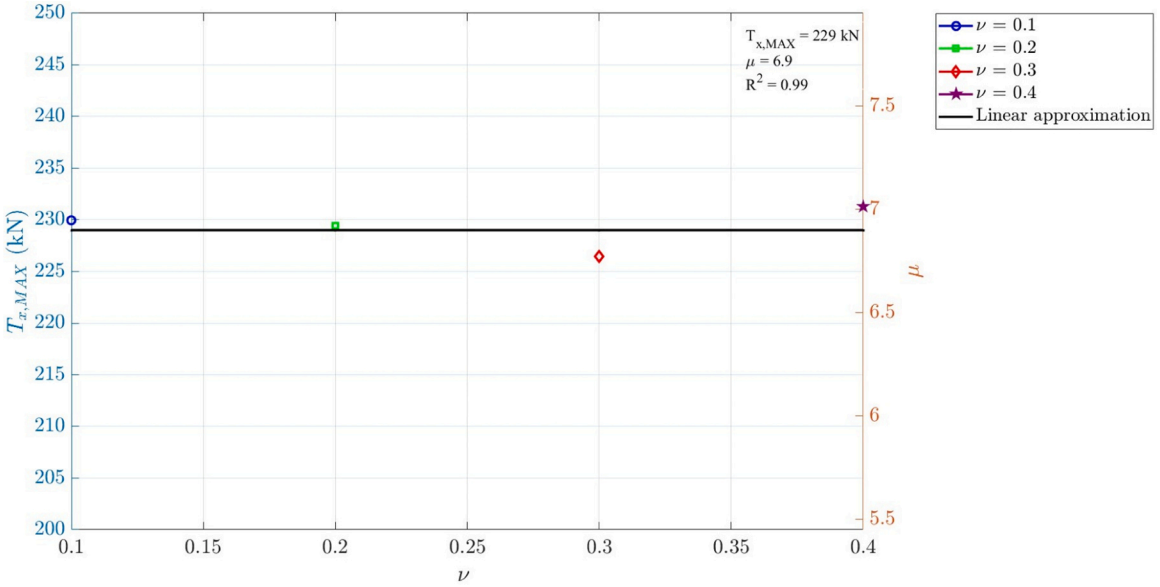

Fig. 22. Sensitivity analysis of Poisson factor.

Fig. 21 the values of the frame ductility μ (calculated in accordance with Eq. 5) have also been plotted, showing μ not to depend on f_t.

Referring to the reduced influence of ν on the calculated value of $T_{x,MAX}$ and μ, it can be observed that the concrete Poisson ratio would have an effect in case of concrete beam-column joint provided of specific reinforcement able to provide an adequate confinement to the compressed concrete. In this case, the assumption of higher ν values would correspond to incremented compressive strengths and deformation limits for the concrete with subsequent better performances of the RC frames both in terms of maximum shear capacity and ductility. In case of unreinforced concrete beam-column joints, as assumed in this study, the lateral expansion of the compressed concrete is not restrained by any specific reinforcement able to provide an effective confinement action, so that no beneficial effects are noticed when higher values are assumed for the Poisson ratio ν.

Data plotted in graph of Fig. 22 show the maximum shear capacity $T_{x,MAX}$ do not depend from the values of the Poisson ratio ν assumed in the numerical analyses of this study and made to vary from 0.1 N/mm^2 to 0.4 N/mm^2. In the same Fig. 22 the values of the Poisson ratio ν have also been plotted, showing ν not to have any influence on μ.

4. Conclusion

An experimental campaign has been carried out to investigate the behavior of RC beam-column wall joints subjected to extreme cyclic loads. The specimens are representative of the existing old structures, in which no shear reinforcements are often found in the joints.

Numerical simulations have also been performed in order to reproduce the experimental cyclic tests and to investigate how the structural behavior of RC beam-column joints depends on several concrete mechanical parameters including: the compressive strength f_c, the tensile strength f_{ctm}, the Young's modulus E_{cm}, the Poisson factor ν and fracture energy in tension G^1.

Although the tested beam-column joints did not include any type of

shear reinforcement, all the tested specimens showed a surprisingly high structural ductility. In particular, experimental shear capacity of the frames did not reduce below 85 % of the maximum response even at drift larger than 4.7 %. Concurrently, numerical simulations confirmed that numerical models may help reproducing the experimental force-displacement curves both in terms of initial stiffness and maximum strength capacity.

Response curves referring to various concrete strength classes highlighted both the computed and experimental maximum shear response and the lateral displacement capacity of the specimens to decrease as the concrete class decreases. In particular, the calculated system capacity reduced by 37.17 % for the concrete class reducing from C40/50 to C20/25.

Numerical models were found to slightly underestimate the displacement $D_{Tx,MAX}$ at which the maximum response is recorded, with experimental $D_{Tx,MAX}$ values representing about 170 % of the calculated ones for the same concrete class.

About the RC frame ductility, the failure of RC beam-column joints is generally considered to be highly brittle. Defining an appropriate ductility factor μ, as done in Eq. 5, allows to better compare the performance of RC frames even in case unreinforced beam-column joints. Both experimental evidence (Fig. 6) and values of μ obtained from numerical simulation, actually prove the ductility of the RC frames in which beam-column joints do not include any specific shear reinforcement, to be significant. This may suggest the adoption of proper behavior factors in the seismic assessment of the existing RC structures so far considered very brittle instead. Numerical data show that as the concrete class increases the ductility factor μ also increases, ranging from a minimum value of $\mu = 6$ (calculated for the concrete class C20/25) to a maximum of $\mu = 8.27$ (calculated for the concrete class C40/50). Experimental ductility values μ_{exp} determined from real tests were found to be even higher then computed ones μ.

Calculated stress distribution in the RC beam-column joint (both for the concrete and the steel rebars) showed the joint failure mode to depend from the assumed value for f_c.

In particular, in case of low concrete strength the frame failure mostly results in shear mode as the compressed strut is wider. Reversely, for higher concrete strength class pressure-bending failure occurs in the joint and the compressed strut is slimmer. These findings are relatively new with respect of the literature because even in the most recent research works the width strut is always assumed to be constant.

In addition, the calculated stresses acting on the reinforcement steel bars at a step analysis at which the maximum response $T_{x,MAX}$ is reached, high- lighted the largest stress to be always located in the longitudinal reinforcement of the beam near the joint rather in the joint itself.

In case of relatively low f_c values (C20/25) the reinforcing bars remained elastic while in all the other cases longitudinal reinforcement of the beam always plasticized near the joint.

This result clearly highlights that favorable structural response (with plastic hinges forming on beams rather in the beam-column joints) may develops also in RC frames built with no shear reinforcement in the joint.

At last, numerical analyses carried out in this study showed the maximum shear strength capacity $T_{x,MAX}$ and the ductility of the system to increase as G^1 increases and equations have been provided to describe these relationships. On the other hand the maximum shear capacity $T_{x,MAX}$ was found not to depends on the values of both the concrete tensile strength and the Poisson ratio respectively.

Funding

This work was carried out as part of the DPC-ReLUIS 2022–2024 research project funded by the Department of Civil Protection.

CRediT authorship contribution statement

Amedeo Gregori: Writing – review & editing, Visualization, Supervision, Methodology, Investigation, Formal analysis, Conceptualization. **Lorenzo Bizzarri:** Writing – original draft, Software, Formal analysis, Data curation, Conceptualization. **D'Agostino Caterina:** Writing – review & editing, Software, Formal analysis.

Declaration of Competing Interest

The authors declare that they have no known competing financial interests or personal relationships that could have appeared to influence the work reported in this paper.

References

[1] Lee J-Y, Kim J-Y, Oh G-J. Strength deterioration of reinforced concrete beam–column joints subjected to cyclic loading. Eng Struct 2009;31(9):2070–85.
[2] Belleri A, Torquati M, Riva P, et al. Valutazione dell'influenza delle connessioni a cerniera di nodi trave-pilastro nell'analisi di vulnerabilita'di struttura prefabbricate. In: Proceedings of the Atti 19° Congresso CTE, Bologna, 8-10 novembre 2012. Universita` degli Studi di Bologna; 2012.
[3] Hanson NW, Connor HW. Seismic resistance of reinforced concrete beam-column joints. J Struct Div, 93; 1967. p. 533–60.
[4] A. C. Institute, Aci 352r-76; (1976).
[5] S. N. Zealand, Concrete structures standard nzs3101:19822; (1982).
[6] Engindeniz M, Kahn LF, Abdul-Hamid Z. Repair and strengthening of reinforced concrete beam-column joints: state of the art. Acids Struct J 2005;102(2):1.
[7] Lowes LN, Altoontash A. Modeling reinforced-concrete beam-column joints subjected to cyclic loading. J Struct Eng 2003;129(12):1686–97.
[8] Zia A, Pu Z, Holly I, Umar T, Tariq MAUR. Development of an analytical model for the frp retrofitted deficient interior reinforced concrete beam-column joints. Appl Sci 2022;12(5):2339.
[9] Lin C-M, Restrepo JI. Seismic behaviour and design of reinforced concrete interior beam-column joints. Bull NZ Soc Earthq Eng 2002;35(2):108–28.
[10] Calvi GM, Magenes G, Pampanin S. Relevance of beam-column joint damage and collapse in rc frame assessment. J Earthq Eng 2002;6(spec01):75–100.
[11] C. Lima, E. Martinelli, C. Faella, Validazione sperimentale di modelli di capacita` per nodi interni trave-colonna di strutture in cemento armato, in: Atti del 18 Congresso CTE, Brescia, 2010, pp. 11–13.
[12] Ricci P, De Luca F, Verderame GM. 6th April 2009 l'aquila earthquake, Italy: reinforced concrete building performance. Bulletin of earth- quake engineering, 9; 2011. p. 285–305.
[13] Beschi C, Riva P, Metelli G, Meda A. Hpfrc jacketing of non seismically detailed rc corner joints. J Earthq Eng 2015;19(1):25–47.
[14] Hakuto S, Park R, Tanaka H. Seismic load tests on interior and exterior beam-column joints with substandard reinforcing details. Struct J 2000;97(1):11–25.
[15] Hassan WM, Moehle JP. Experimental assessment of seismic vulnerability of corner beam-column joints in older concrete buildings. Proc 15th World Conf Earthq Eng 2012;9.
[16] Masi A, Santarsiero G, Nigro D. Cyclic tests on external rc beam-column joints: role of seismic design level and axial load value on the ultimate capacity. J Earthq Eng 2013;17(1):110–36.
[17] Murad Y, Abdel-Jabar H, Diab A, Abu Hajar H. Exterior rc joints subjected to monotonic and cyclic loading. Eng Comput 2020;37(7):2319–36.
[18] Sharma A, Reddy G, Vaze K, Eligehausen R. Pushover experiment and analysis of a full scale non-seismically detailed rc structure. Eng Struct 2013;46:218–33.
[19] Beres A, El-Borgi S, White RN, Gergely P. Experimental results of repaired and retrofitted beam-column joint tests in lightly reinforced concrete frame buildings. Technical Rep. No. NCEER-92 1992:25.
[20] L.-p Ye, X.-l Jin, Y. Tian, X.-z Lu, Z.-w Miao, Z. Qu, , "system capacity design method" for the seismic design of building structures: a review, 39 (5) (2022) 1–12.
[21] Fardis MN. Capacity design: early history. Earthq Eng Struct Dyn 2018;47(14):2887–96.
[22] MIT, C.m. 10-4-1997; (1997).
[23] MIT, Norme tecniche per le costruzioni 2008; (2008).
[24] MIT, Norme tecniche per le costruzioni 2018; (2018).
[25] Castorina R, Pitzalis S. Comprendere I disastri. Linee teoriche e applicazioni metodologiche della socio-antropologia nei terremoti de l'aquila e dell'emilia. Argomenti 2019;12:7–36.
[26] J.I. Braverman, C.A. Miller, B.R. Ellingwood, D.J. Naus, C.H. Hofmayer, P. Bezler, , Structural performance of degraded reinforced concrete members; (2001).
[27] Fardis MN. Shear strength model for rc joints, consistent with the shear design rules for prismatic members in the second-generation eurocodes. Bull Earthq Eng 2021;19(2):889–917.
[28] Gregori A, Bizzarri L, D'Agostino C, Aloisio A, Cirella R, Alaggio R. Sensitivity analysis of modal parameters of an rc joint subject to progressive damage under cyclic loads. Buildings 2024;14(5):1345.
[29] Gregori A, Castoro C, Di Natale A, Mercuri M, Di Giampaolo E. Using commercial uhfrfid wireless tags to detect structural damage. Procedia Struct Integr 2023;44:1586–93.
[30] F. internationale du bèton (FIB), Cebfib model code for concrete structures; (2020).
[31] A. C. Institute, Guide for the evaluation of concrete structures subjected to earthquake ground shaking; (2005).

[32] Nicoletti V, Carbonari S, Gara F. Nomograms for the pre-dimensioning of rc beam-column joints according to eurocode 8. In: Structures, 39. Elsevier; 2022. p. 958–73.
[33] Asgarpoor M, Gharavi A, Epackachi S. Investigation of various concrete materials to simulate seismic response of rc structures. In: Structures, 29. Elsevier; 2021. p. 1322–51.
[34] Di Carlo F, Meda A, Rinaldi Z. Numerical cyclic behaviour of uncorroded and corroded rc columns reinforced with hpfrc jacket. Compos Struct 2017;163: 432–43.
[35] Earij A, Alfano G, Cashell K, Zhou X. Nonlinear three–dimensional finite–element modelling of reinforced–concrete beams: computational challenges and experimental validation. Eng Fail Anal 2017;82:92–115.
[36] Lima C, Angiolilli M, Barbagallo F, Belletti B, Bergami A, Camata G, et al. Nonlinear modeling approaches for existing reinforced concrete build- ings: the case study of de gasperi-battaglia school building in norcia. In: Proceedings of the Italian concrete days 2018. Springer; 2020. p. 82–95.
[37] Angiolilli M, Gregori A, Tonelli R, Tonelli C, Ciuffetelli E, Peditto A. Structural performance of unreinforced full-scale fa¸cade concrete beam-column joint under cyclic load. Procedia Struct Integr 2023;44:870–7.
[38] Angiolilli M, Gregori A, Bizzarri L, D'Agostino C, Ciuffetelli E, Peditto A, et al. Nuumerical modelling of poorly detailed existing rc beam-column joints. Compdyn Proc 2023.
[39] Lima C, Martinelli E, Faella C. Capacity models for shear strength of exterior joints in rc frames: state-of-the-art and synoptic examination. Bull Earthq Eng 2012;10: 967–83.
[40] Fajfar P. A nonlinear analysis method for performance-based seismic design. Earthq Spectra 2000;16(3):573–92.
[41] Bisch P, Carvalho E, Degee H, Fajfar P, Fardis M, Franchin P, et al. Eurocode 8: seismic design of buildings worked examples. Luxembourg: Publications Office of the European Union; 2012.